Ethylene Epoxidation on Ag(110): The Role of Subsurface Oxygen

P. J. van den Hoek,*

FOM Institute for Atomic and Molecular Physics, Kruislaan 407, 1098 SJ Amsterdam, The Netherlands

E. J. Baerends,*

Department of Theoretical Chemistry, Free University of Amsterdam, De Boelelaan 1083, 1081 HV Amsterdam, The Netherlands

and R. A. van Santen

Department of Inorganic Chemistry and Catalysis, Technical University of Eindhoven, P.O. Box 513, 5600 MB Eindhoven, The Netherlands *(Received: December 15, 1988; In Final Form: March 23, 1989)*

We have performed electronic structure calculations on the chemisorption of atomic oxygen on Ag(110) and on the subsequent reaction of this chemisorbed oxygen with ethylene. These calculations show that the presence of subsurface oxygen (i) reduces the bond energy between silver and adsorbed oxygen and (ii) converts the *repulsive* interaction between adsorbed oxygen and (gas-phase) ethylene into an *attractive* one, thus making possible the epoxidation reaction. The presence of subsurface oxygen diminishes an important four-electron destabilizing interaction (Pauli repulsion) between the occupied ethylene π orbital and a surface oxygen lone-pair orbital by shifting the band of ethylene π–oxygen lone-pair antibonding orbitals largely above the Fermi level. As for total combustion of ethylene, we do not find any C–H bond activation for several different geometries in which ethylene approaches the adsorbed oxygen atom.

1. Introduction

The epoxidation of ethylene over the surface of a silver catalyst is an important reaction in industry. Apart from epoxide formation, in which an oxygen atom is inserted in the carbon–carbon double bond of ethylene, combustion can also take place, in which the ethylene is converted into CO_2 and H_2O. During the past 20 years, much experimental research has been devoted to getting a better understanding of the epoxidation reaction,[1] with the ultimate goal to be able to increase the selectivity for epoxide formation. This has led to a fairly good insight into the mechanism for ethylene epoxidation.[1] Here, we briefly summarize the most important features:

(1) Ethylene reacts with adsorbed *atomic* oxygen to epoxide.

(2) Once the adsorbed atomic oxygen has been formed, the rate-limiting step for epoxidation is the insertion of this oxygen into the C–C double bond. The rate-limiting step for combustion is probably a C–H bond activation,[2] although C–C bond activation cannot be definitely excluded.[3] We will come back to this point later.

(3) *Subsurface* oxygen (or other moderators, e.g., chlorine) seems to be necessary for adsorbed oxygen to react to epoxide.[1,4] These subsurface species are stabilized by alkali-metal atoms,[5] which explains why also alkali-metal promotors enhance the selectivity.

(4) From points 1 and 2, it follows why silver is taken as a catalyst: it has the ability to dissociate oxygen,[6,7] but at the same time cannot activate C–H (or possibly C–C) bonds, since it has no open d shell.[1]

The fact that subsurface O or Cl is necessary for epoxide formation is one of the most important features of the epoxidation reaction which is still poorly understood. One generally assumes that subsurface O weakens the chemisorption bond of adsorbed atomic O, thus making it easier to transfer to ethylene. Recently, Carter et al. suggested that, on Ag(110), moderators in general promote the formation of a chemically active "surface atomic oxy radical",[8] by blocking the adsorption sites for inactive "di-σ" oxygen in the troughs along the [1$\bar{1}$0] direction. These authors, however, did not consider the effect of subsurface oxygen. In this work we use electronic structure calculations, in which the Ag(110) surface is modeled by finite clusters, to show that subsurface oxygen indeed weakens the bond of oxygen which is chemisorbed in the troughs along the [1$\bar{1}$0] direction. In addition, however, subsurface oxygen increases the binding energy between adsorbed oxygen and (gas-phase) ethylene: whereas in the absence of subsurface oxygen this interaction is *repulsive*, it becomes *attractive* in the presence of subsurface oxygen. As a consequence of these two effects, the barrier for reaction to epoxide disappears. An explanation is given both for the oxygen chemisorption bond weakening and the oxygen–ethylene bond strengthening due to subsurface oxygen. As for combustion, we find no C–H bond activation for several different geometries of ethylene approaching the adsorbed oxygen atom. On the basis of our results, C–C bond activation cannot be excluded.

The paper is organized as follows. Section 2 gives an outline of the computational details and a description of the model clusters. In section 3, results are presented and discussed. Section 3.1 discusses the influence of subsurface O on the bond energy of adsorbed O. In section 3.2, the reaction of adsorbed O with ethylene, leading to epoxide, is discussed. In section 3.3, possibilities for combustion are considered. Finally, section 4 gives conclusions.

2. Method

2.1. General. Calculations were performed using the Hartree–Fock–Slater linear combination of atomic orbitals (HFS-LCAO) method.[9] The local Xα exchange functional was used, $\alpha = 0.7$. Interaction energies were calculated according to a transition-state method.[10] We used standard[11] (double-ζ) Slater type orbital (STO) basis sets, together with a d function, for the

(1) For a recent review, see: van Santen, R. A.; Kuipers, H. P. C. E. In *Advances in Catalysis*; Academic Press: New York, 1987; Vol. 35, p 265.
(2) Cant, N. W.; Hall, W. R. *J. Catal.* **1978**, *52*, 81. van Santen, R. A.; Moolhuysen, J.; Sachtler, W. M. H. *J. Catal.* **1980**, *65*, 478. Grant, R. B.; Lambert, R. M. *J. Catal.* **1985**, *92*, 364.
(3) Twigg, G. H. *Trans. Faraday Soc.* **1946**, *42*, 284. Klugherz, P. D.; Harriott, P. *AIChE J. 17*, **1971**, 856.
(4) Backx, C.; Moolhuysen, J.; Geenen, P.; van Santen, R. A. *J. Catal.* **1981**, *72*, 364. Grant, R. B.; Lambert, R. M. *J. Chem. Soc., Chem. Commun.* **1983**, 662. van Santen, R. A.; de Groot, C. P. M. *J. Catal.* **1986**, *98*, 530.
(5) van Santen, R. A. *Proceedings of the 9th International Congress on Catalysis, Calgary*, **1988**; Phillips, M. J., Ternan, M., Eds.; The Chemical Institute of Canada: Ottawa, 1988.
(6) Campbell, C. T. *Surf. Sci.* **1985**, *157*, 43.
(7) van den Hoek, P. J.; Baerends, E. J. To be published.
(8) Carter, E. A.; Goddard, W. A., III *J. Catal.* **1988**, *112*, 80.
(9) Baerends, E. J.; Ellis, D. E.; Ros, P. *Chem. Phys.* **1973**, *2*, 41.
(10) Ziegler, T.; Rauk, A. *Theor. Chim. Acta* **1973**, *46*, 1.
(11) Snijders, J. G.; Vernooijs, P.; Baerends, E. J. *At. Data Nucl. Data Tables* **1981**, *26*, 483; Internal Report [Free University, Amsterdam, 1981 (unpublished)].

0022-3654/89/2093-6469$01.50/0

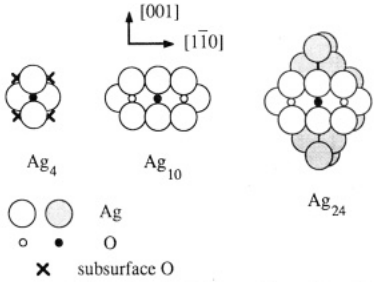

Figure 1. Clusters modeling the Ag(110) surface. The shaded Ag atoms have a frozen 4d orbital. The positions of the four subsurface atoms (at the height of the second layer) are indicated by crosses for the Ag_4 cluster.

oxygen and carbon atoms. Here, the 1s core orbitals were kept frozen. For hydrogen, a double-ζ basis set with a 2p polarization function was used. In the case of silver, we used both a basis set in which the 4d orbital was unfrozen and one in which it was frozen (see next section). In both cases, all core orbitals up to the 4p orbital were kept frozen. The silver basis sets (triple-ζ, and a 5p polarization function) were separately optimized.[12]

2.2. Clusters. We approximated the Ag(110) surface by Ag_4, Ag_{10}, and Ag_{24} clusters. Figure 1 shows the three different silver clusters. In the Ag_{24} cluster, the 4d orbitals of the shaded Ag atoms are frozen; the other Ag atoms have unfrozen 4d orbitals. In Ag_4 and Ag_{10}, all Ag atoms have unfrozen 4d orbitals. The largest system on which we performed calculations (Ag_{24} + 6O, see below) contained 1014 basis functions. Our Ag_{24} cluster is the same as that used by Upton et al.,[13] who performed calculations on the chemisorption of molecular oxygen on Ag(110); the only difference is that these authors employed unfrozen 4d orbitals only for the four central Ag atoms.[13] Experiments suggest that for coverages $\leq$0.5 monolayer, the oxygen atoms occupy the bridge sites in the troughs along the [1$\bar{1}$0] direction.[15] Therefore, for all three clusters (Ag_4, Ag_{10}, and Ag_{24}), we considered the chemisorption of one oxygen atom at the central site in the trough (filled oxygen atoms in Figure 1). For the Ag_{10} and Ag_{24} clusters, we also considered the simultaneous chemisorption of two oxygen atoms in the trough (Figure 1, open oxygen atoms). The latter configuration corresponds to an oxygen coverage of 0.5 monolayer. This configuration was studied in order to see whether the influence of subsurface oxygen is dependent on oxygen coverage. The reaction of chemisorbed oxygen with (gas-phase) ethylene was only considered for the Ag_4 cluster and for the Ag_{10} cluster with two chemisorbed oxygen atoms. A more detailed description of the different geometries in which the ethylene approaches the adsorbed oxygen is given in sections 3.2 and 3.3.

Nothing is known experimentally about the position of subsurface oxygen. We put four oxygen atoms at high-symmetry open sites in the second layer, as indicated for the Ag_4 cluster (crosses); for all clusters, we used these four subsurface atoms. In bulk silver, such a subsurface oxygen atom will be 6-fold coordinated, with a nearest-neighbor Ag–O distance close to that of bulk Ag_2O (2 Å).

3. Results and Discussion

3.1. Chemisorption of Atomic Oxygen. In this section, we discuss the influence of subsurface oxygen on the chemisorption of atomic oxygen on the surface. We start by considering oxygen adsorption in the absence of subsurface oxygen. Table Ia shows the calculated bond energies D_e (per adsorbed O atom), equilibrium distances above the surface r_e, shortest Ag–O distances d(Ag–O), and vibrational frequencies ω_e as function of cluster size (4, 10, or 24) and adsorption site on the cluster (one O atom or two O atoms; see section 2.2). Also, experimental values and results from other calculations are shown. The calculated binding energies exhibit the well-known oscillation with cluster size,[19] but in general, there is a reasonable agreement between our calculations and experiment. Note, that there is a large difference in D_e between our results (and the experimental results) and those of Martin and Hay,[17] the reason for which is not completely clear (cf. the comments in ref 17). With the exception of Ag_{10} + O, all binding energies are somewhat too high, but this is a general property of Xα-type calculations.[20] Now, let us see how the oxygen bonds to the silver surface. Figure 2a shows the partial density of states (PDOS) of the p orbitals of the chemisorbed oxygen atoms for the case of Ag_{10} + 2O. Two main structures are seen which straddle the Ag(4d) band (see Figure 3). As expected,[17,21] the lower one is O(2p)/Ag(4d) bonding, the higher one O(2p)/Ag(4d) antibonding. This may be seen from the crystal orbital overlap population (COOP)[22] between the O 2p and the silver orbitals (Figure 2b). The COOP gives the (anti-) bonding character of the states in the PDOS: a positive COOP means bonding states and a negative COOP antibonding states. The COOP curves in Figure 2b show clearly O(2p)/Ag(4d) bonding (antibonding) character in the low (high) energy structures. The O(2p)/Ag(4d) bonding peak is ca. 1.5 eV below the center of the 4d band (not drawn in Figure 2a; see Figure 3a), in reasonable agreement with photoemission experiments.[23] Note that most of the O(2p) character is present in the broad O(2p)/Ag(4d) antibonding structure just below the Fermi level E_F (in agreement with previous calculations[17,21]), which is in contrast with the situation for bulk Ag_2O, where most of the O(2p) character is in the lower (bonding) structure[24] [another difference with Ag_2O is that the silver–subsurface oxygen system is metallic (nonzero total DOS at E_F; see Figure 3b), contrary to Ag_2O[24]]. Clearly, net bonding with Ag(4d) will not be large since most of the antibonding structure is below E_F. The Ag sp states, however, which form a broad band extending to much higher energy than

TABLE I: Calculated D_e (Chemisorption Energy), r_e (Equilibrium Distance above the Surface), and ω_e (Vibrational Frequency) for Oxygen Adsorption on Silver Clusters Representing Ag(110), as a Function of Cluster Size and Adsorption Site on the Clusters (See Text)

	D_e, eV	r_e, Å	d(Ag–O), Å	ω_e, cm^{-1}
	(a) Without Subsurface Oxygen			
Ag_4 + O	4.39	0.33	2.07	286
Ag_{10} + O	2.84	0.34	2.07	257
Ag_{10} + 2O	3.54	0.38	2.08	223
Ag_{24} + O	3.79	0.49	2.10	265
Ag_{24} + 2O	4.12	0.48	2.10	267
expt	3.47[a]	$0.0^{+0.7}_{-2.0}$[b]	$2.04^{+0.7}_{-2.0}$[b]	310, 325[c]
other calcns				
ref 17	0.39	0.29	2.08	325
ref 18		0.26	2.06	400
	(b) With Subsurface Oxygen			
Ag_4 + O	2.58	0.53	2.11	235
Ag_{10} + O	1.53			
Ag_{10} + 2O	3.18	0.65	2.14	184
Ag_{24} + O	3.21			
Ag_{24} + 2O	2.75	0.64	2.14	262

[a] Reference 14. [b] Reference 15. [c] Reference 16.

(12) van den Hoek, P. J. Unpublished results.
(13) Upton, T. H.; Stevens, P.; Madix, R. J. *J. Chem. Phys.* **1988**, *88*, 3988.
(14) Engelhardt, H. A.; Menzel, D. *Surf. Sci.* **1976**, *57*, 591.
(15) Heiland, W.; Iberl, F.; Taglauer, E.; Menzel, D. *Surf. Sci.* **1975**, *53*, 383.
(16) Sexton, B. A.; Madix, R. J. *Chem. Phys. Lett.* **1980**, *76*, 294. Backx, C.; de Groot, C. P. M.; Biloen, P. *Appl. Surf. Sci.* **1980**, *6*, 256.
(17) Martin, R. L.; Hay, P. J. *Surf. Sci.* **1983**, *130*, L283.
(18) Selmani, A.; Anzelm, J.; Salahub, D. R. *Int. J. Quantum Chem.* **1986**, *29*, 829.
(19) Post, D.; Baerends, E. J. *J. Chem. Phys.* **1983**, *78*, 5663. Hermann, K.; Bagus, P.; Nelin, C. *Phys. Rev. B* **1987**, *35*, 9467.
(20) Painter, G. S.; Averill, W. *Phys. Rev. B* **1983**, *26*, 1781.
(21) Rosch, N.; Menzel, D. *Chem. Phys.* **1976**, *13*, 243.
(22) Hoffmann, R.; Zheng, C. *Proceedings of the NATO Advanced Research Workshop and 40th International Meeting of the Societe du Chimie Physique, Strasbourg, France, September 16–20, 1985*; Veillard, A., Ed.; Reidel: Dordrecht, Holland, 1986; p 425.
(23) Prince, K. C.; Bradshaw, A. M. *Surf. Sci.* **1983**, *126*, 49.
(24) Czyzyk, M. Unpublished results.

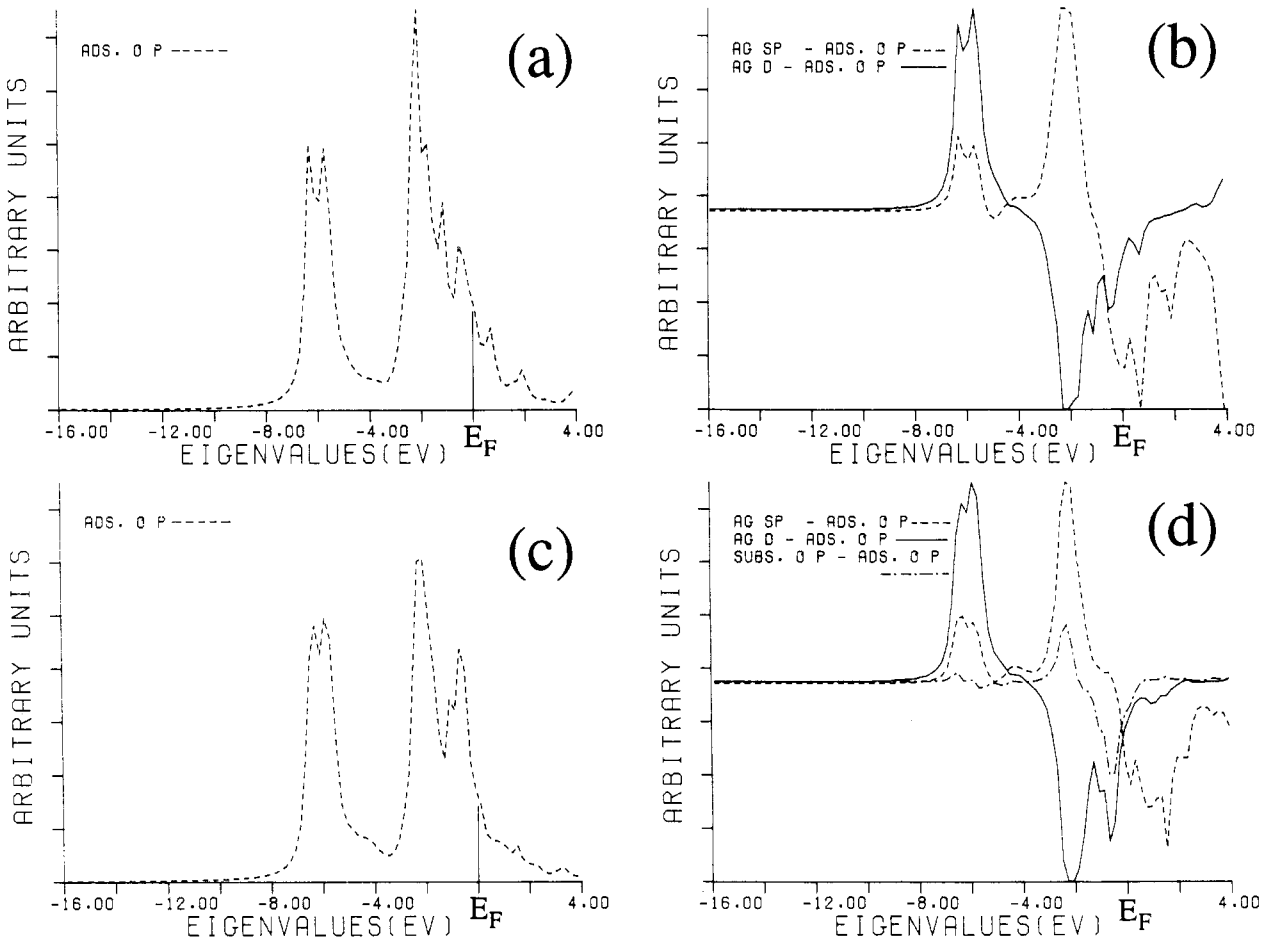

Figure 2. (a and c) PDOS curves of the p orbitals of oxygen chemisorbed on Ag(110) without (a) and with (c) subsurface oxygen. (b and d) COOP curves of the interactions between chemisorbed oxygen p orbitals, and silver and subsurface oxygen orbitals, without (b) and with (d) subsurface oxygen. The interactions with the silver d band (solid), sp band (dashed), and subsurface oxygen band (dot–dashed) are shown. The curves are based on calculations with Ag_{10}.

the silver 4d band (see Figure 3a), mix into the O(2p) orbitals in a bonding manner, particularly into the O(2p)/Ag(4d) antibonding band, but also to some extent into the O(2p)/Ag(4d) bonding levels (Figure 2b). The strong positive COOP with Ag sp almost cancels the negative contribution from Ag(4d) in the high-energy band. From the PDOS and COOP curves in parts a and b of Figure 2, we can derive a qualitative interaction diagram for atomic oxygen chemisorption on silver, as depicted in Figure 4a. In this diagram, for simplicity, the silver d and sp bands are indicated by discrete levels. As indicated, the silver–oxygen interaction leads to a low-lying level due to bonding with the d band and a level closer to (but still below) E_F which is approximately oxygen–silver nonbonding, due to a cancellation of the interactions with the d band and sp band.

As a next step, we consider atomic oxygen chemisorption in the presence of subsurface oxygen. Table Ib shows D_e, r_e, and ω_e in this case for the different clusters and chemisorption sites. For Ag_{10} + O and Ag_{24} + O, we did not optimize the bond distance, but instead evaluated the bond energy for r = 0.8 Å, which is expected to be reasonably close to r_e. From a comparison of Table Ia and Table Ib, we clearly see a weakening of the chemisorption bond due to subsurface oxygen: D_e and ω_e decrease and r_e increases. In order to understand this bond weakening, we first have to see what happens with the silver states when subsurface oxygen is incorporated. Figure 3 shows for Ag_{10} the PDOS in the absence (a) and presence (b) of subsurface oxygen. The PDOS of Figure 3a is what one expects for pure silver: a localized d-band well below E_F, and a delocalized (broadened) s band around E_F. The incorporation of subsurface oxygen leads to the formation of new states at the lower edge of the d band and above the d band, just below the Fermi level. These states are completely analogous to the ones we found for adsorbed oxygen before. The structure just below E_F is mostly (subsurface) oxygen 2p but also contains considerable Ag 4d and 5sp character. What happens when oxygen is adsorbed? Figure 2c shows the PDOS of the 2p states of adsorbed oxygen in the presence of subsurface oxygen. When we compare this figure with Figure 2a, we see that also in this case there are pronounced structures at ~6 eV and ~2 eV below E_F. From the COOP in Figure 2d, we see that the structure at ~6 eV below E_F is due to a bonding interaction with the d band, just as in the absence of subsurface oxygen. Similarly, the structure at ~2 eV blow E_F is largely oxygen–silver nonbonding due to the cancellation we discussed earlier. In addition, this structure is somewhat (adsorbed oxygen)–(subsurface oxygen) bonding. The clear difference, however, from Figure 2a is that now there is a *third* structure at ~0.6 eV below E_F. This structure is clearly O(2p)/Ag(4d) antibonding as we can see from Figure 2d. Also, this structure is (adsorbed oxygen)–(subsurface oxygen) antibonding. Apparently, the incorporation of subsurface oxygen leads to a clear splitting of the original band of O(2p)/Ag(4d) antibonding states in a two-peak structure of states that are bonding and antibonding with respect to subsurface oxygen. Since both bonding and antibonding states are occupied (below E_F), this leads to a weakening of the chemisorption bond. Figure 2c and Figure 2d are summarized in the qualitative interaction diagram of Figure 4b. In the presence of subsurface oxygen, there is a third band of mainly subsurface O(2p) character between the silver d and s bands; this is indicated to the left. The interaction of adsorbed oxygen with this band leads to bonding and antibonding levels, both below E_F; this results in the weakening of the oxygen chemisorption bond just mentioned.

The states in the band at 0.6 eV below E_F play a crucial role in the interaction between adsorbed oxygen and ethylene in the presence of subsurface oxygen, as we will show in the next section.

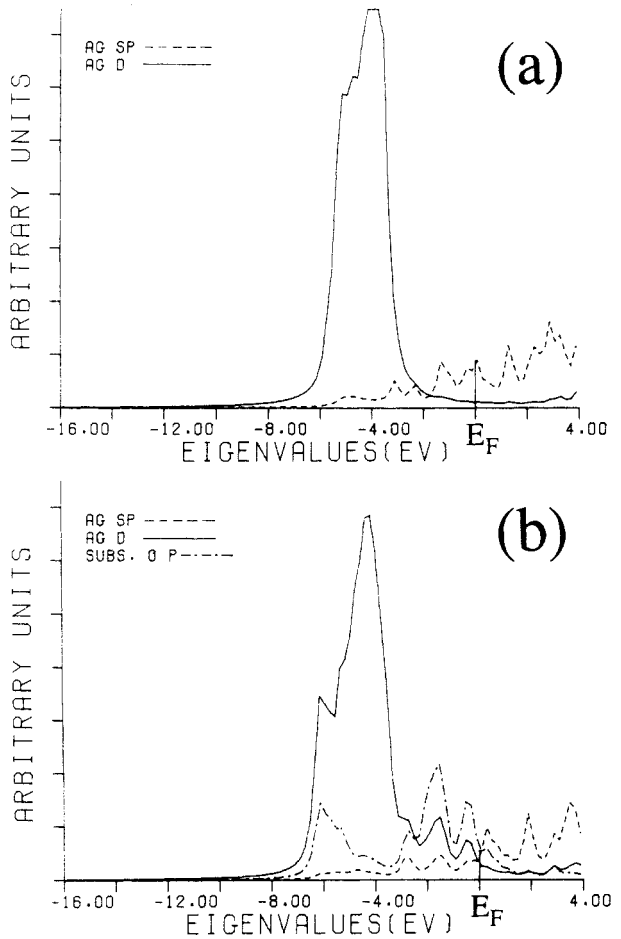

Figure 3. PDOS curves of the silver sp (dashed) and d bands (solid) without (a) and with (b) subsurface oxygen. In (b) the PDOS of the subsurface oxygen p orbitals is also drawn. The curves are based on calculations with Ag_{10}.

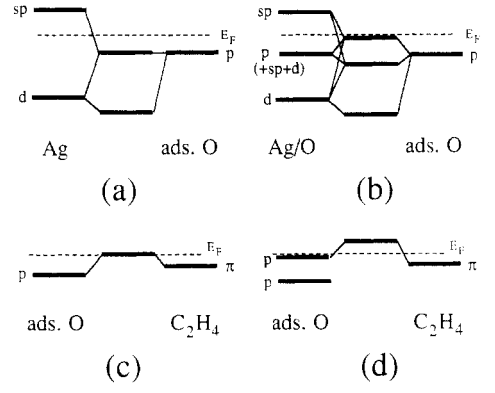

Figure 4. Schematical interaction diagrams of the chemisorption of oxygen on silver [(a and b)] and of the interaction between this oxygen and ethylene in the geometry for epoxidation [(c and d)]. Silver without [(a and c)] and with [(b and d)] subsurface oxygen is considered. The diagrams have been derived from the PDOS and COOP curves in Figure 3.

Figure 5 shows a plot of the spatial distribution of one of the orbitals in this band. The orbital is plotted in two different planes: the plane defined by the adsorbed oxygen atom and the surface Ag atoms (Figure 5a) and the plane defined by adsorbed and subsurface oxygen atoms (Figure 5b). Clearly, this orbital is both O(2p)/Ag(4d) (Figure 5a) and O(2p)/O(2p) (Figure 5b) antibonding. In order to "lower" the antibonding character, the adsorbed $O(2p_z)$ amplitude pointing out of the silver surface (that is, away from the Ag(4d) and the subsurface O) is increased by mixing in of the O(2s) orbital, resulting in a pronounced hybridized lone-pair orbital; this can also be seen in Figure 5. Both the

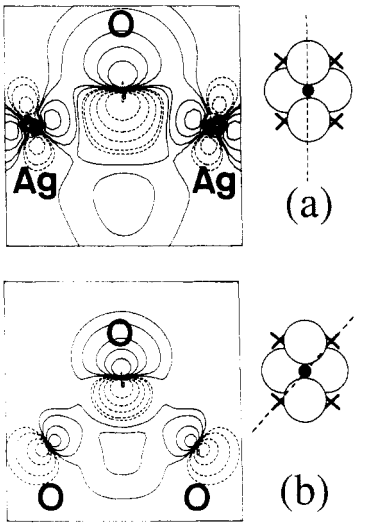

Figure 5. Orbital plots of one of the orbitals in the structure ~0.6 eV below E_F when subsurface oxygen is present (see Figure 2c,d). (a) The orbital is plotted in the plane defined by the chemisorbed oxygen atom (center) and the surface silver atoms, that is, the $(1\bar{1}0)$ plane. (b) The orbital is plotted in the plane defined by the chemisorbed (center) and subsurface oxygen atoms. In both (a) and (b) the [110] direction is pointing upward (z direction). Solid and dashed contours indicate positive and negative values, respectively; contour values are ±0.01, ±0.02, ±0.05, ±0.1, ±0.2, and ±0.5 $a_0^{-3/2}$.

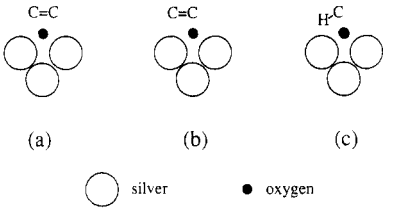

Figure 6. Projected views along the $[1\bar{1}0]$ direction (parallel to the grooves) of the possible geometries of ethylene approach to adsorbed oxygen that were considered in the calculations.

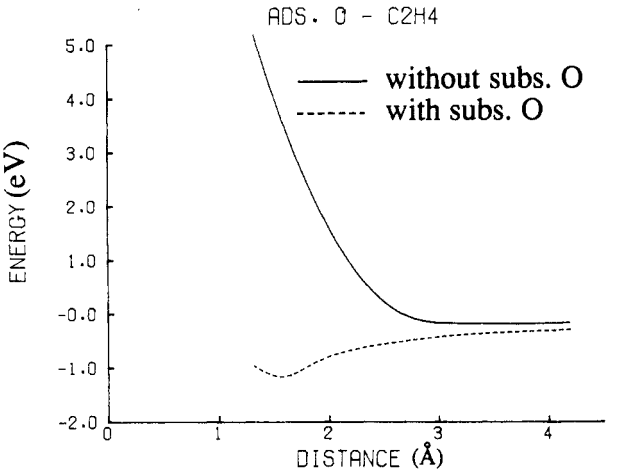

Figure 7. Interaction energy as a function of adsorbed oxygen–ethylene distance for the geometry of Figure 6a without (solid) and with (dashed) subsurface oxygen. The curves are based on calculations with Ag_4.

proximity of the O lone-pair states to E_F and the large amplitude pointing out of the surface, that is, at the side of the incoming ethylene molecule, are important for the epoxidation reaction to be discussed below. Note that the chemisorption bond weakening due to subsurface oxygen has an important *local* component: the subsurface oxygen has to be close to the adsorbed oxygen.

3.2. Symmetric Attack of Ethylene on Oxygen; Epoxidation. In this section we consider the "symmetric" attack of ethylene on chemisorbed oxygen (Figure 6a) and the subsequent reaction to ethylene epoxide. The ethylene approaches the oxygen with

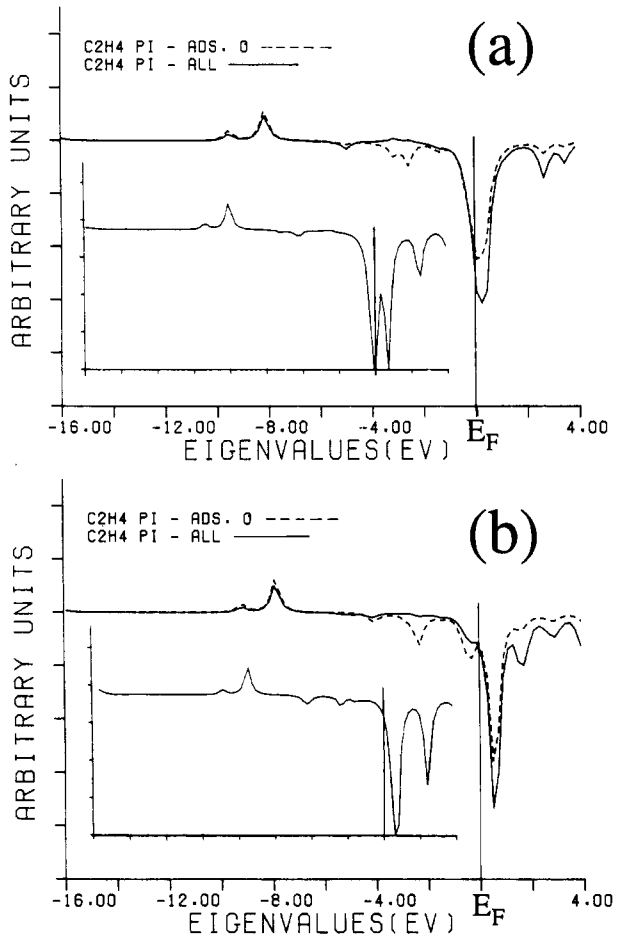

Figure 8. COOP curves of the interaction between silver + adsorbed oxygen and the carbon–carbon π-bond orbital of ethylene for the geometry of Figure 6a, without (a) and with (b) subsurface oxygen. The interactions of ethylene with adsorbed oxygen alone (dashed) and with silver and adsorbed oxygen together (solid) are shown. The curves are based on the calculations with Ag_{10}, with an oxygen–silver surface distance of 0.79 Å and an oxygen–ethylene distance of 1.59 Å. Insets: The same, based on the calculations with Ag_4.

its molecular plane parallel to the silver surface. In principle, this geometry can lead to direct epoxide formation. Figure 7 shows for this geometry the interaction energy between the chemisorbed oxygen and ethylene as a function of the distance between the oxygen and the center of the carbon–carbon bond. This figure is based on calculations with Ag_4. From this figure, we see that, in the absence of subsurface oxygen, the adsorbed oxygen–ethylene interaction is purely repulsive (except for a very small minimum due to polarization of ca. 0.15 eV at 3 Å). The incorporation of subsurface oxygen drastically changes the picture: the *repulsive* interaction is converted into an *attracive* one, with a bond minimum at an oxygen–ethylene distance of about 1.6 Å, slightly larger than the equilibrium distance for ethylene epoxide (~1.3 Å). In the case of the Ag_{10} clusters, for which we consider the approach of ethylene to each of the two adsorbed oxygen atoms (open small circles in Figure 1), we calculate a similar behavior. For example, at the oxygen–ethylene distance of 1.6 Å (which is also the position of the minimum for Ag_{10} with subsurface oxygen), the interaction energies for Ag_4 and Ag_{10} are +1.2 and +0.8 eV, respectively, without subsurface O and −1.2 and −0.7 eV with subsurface O.

With the aid of Figure 8, we can explain this influence of subsurface oxygen on the interaction of ethylene and adsorbed oxygen. In this figure, COOP curves are drawn of the interaction between the (occupied) carbon–carbon π bond in ethylene and the oxygen and silver orbitals, without (Figure 8a) and with (Figure 8b) subsurface oxygen. Both figures are based on calculations, performed with the Ag_{10} clusters, for the same silver–oxygen (0.8 Å) and oxygen–ethylene (1.6 Å) distance. The COOP curves in the two parts of Figure 8 have qualitatively the same shape; in both cases the interaction is mainly a direct oxygen–ethylene interaction (the remaining part of the total COOP is due to interaction with the silver sp band). The main difference between Figure 8a and Figure 8b is that the strongly oxygen–ethylene antibonding structure is partly below E_F in the absence of subsurface oxygen (Figure 8a), whereas it is completely above E_F in the presence of subsurface oxygen (Figure 8b). This is due to the following. In the absence of subsurface oxygen, the $C_2H_4(\pi)$–O(2p) antibonding level is positioned around E_F, as is schematically indicated in Figure 4c. Now, due to the antibonding interaction with subsurface oxygen, part of the adsorbed O(2p) DOS has been "pushed" to higher energies, as we saw in the previous section; these are the O lone-pair orbitals, one of which is depicted in Figure 5. The adsorbed O lone-pair orbitals have, as noted earlier, a large amplitude at the side of the incoming C_2H_4 and will strongly interact with the C_2H_4 π orbital. Due to the proximity to the Fermi level of the O lone-pair orbitals, the C_2H_4–O antibonding levels will be positioned above E_F, as is schematically indicated in Figure 4d. The fact that the C_2H_4–O strongly antibonding levels are partially filled in the absence of subsurface oxygen, whereas they are empty in the presence of subsurface oxygen, results in a stronger C_2H_4–O bond in the latter case. The insets of Figure 8a,b show similar COOP curves based on calculations with the Ag_4 clusters. Also here, we see that the presence of subsurface oxygen depletes the strongly ethylene–oxygen antibonding levels, thus increasing the bond energy.

The simultaneous effect of subsurface oxygen on the silver–adsorbed oxygen bond and on the adsorbed oxygen–ethylene bond is shown in Figure 9. This figure shows contour plots of the potential energy surfaces for reaction to epoxide (geometry of Figure 6a) without (Figure 9a) and with (Figure 9b) subsurface oxygen; the figure is based on calculations with Ag_4. On the horizontal axis the adsorbed oxygen–ethylene distance is given, and on the vertical axis the height of the oxygen above the surface is given. Starting with ethylene and adsorbed oxygen, we enter the figure from the right at $r(Ag–O) \approx 0.5$ Å. If no subsurface O is present, we have to go over a barrier with a height of about 1.5 eV (saddle point in Figure 9a) before epoxide is formed and "leaves the figure" along a vertical line at $r(O–C_2H_4) \approx 1.3$ Å. When subsurface O is present, the barrier for reaction to epoxide completely vanishes, as we can see from Figure 9b: an incoming ethylene molecule directly reacts to epoxide. The calculations with Ag_{10} give similar results: here, the barrier for reaction to epoxide is about equal to 0.9 eV (per ethylene molecule) in the absence of subsurface oxygen, whereas there is no barrier when subsurface oxygen is present.

3.3. Asymmetric Attack of Ethylene on Oxygen; Combustion. In this section, we consider two different geometries of asymmetric attack of ethylene on adsorbed oxygen (Figure 6). In the first geometry, the ethylene approaches the oxygen with its plane parallel to the silver surface, but with one of its carbon atoms directly above the oxygen (Figure 6b). In the second geometry, the ethylene approaches the oxygen with one of its C–H bonds parallel to an O–Ag bond. The geometry of Figure 6b is interesting, since isomerization experiments of isotope-labeled ethylene suggest that epoxide is mostly formed by an attack in this geometry.[25] In addition, in the absence of subsurface oxygen, this geometry could more easily lead to combustion than symmetric (Figure 6a) attack, since both the $C–H^2$ and $C–C^3$ bonds are more easily activated. The geometry of Figure 6c could possibly lead to combustion through C–H bond breaking. In this section, we will focus on possible combustion mechanisms for the geometries of Figure 6b,c in the *absence* of subsurface oxygen. When subsurface oxygen is present, our calculations with the Ag_4 clusters show that the ethylene–oxygen interaction energy for the asymmetric geometry of Figure 6b is about equal to that for symmetric attack (Figure 6b), from which follows that indeed epoxide may be formed by both asymmetric and symmetric attacks.

(25) Egashira, M.; Kuczkowski, R. L.; Cant, N. W. *J. Catal.* **1980**, *65*, 297. Richey, W. F. *J. Phys. Chem.* **1972**, *76*, 213.

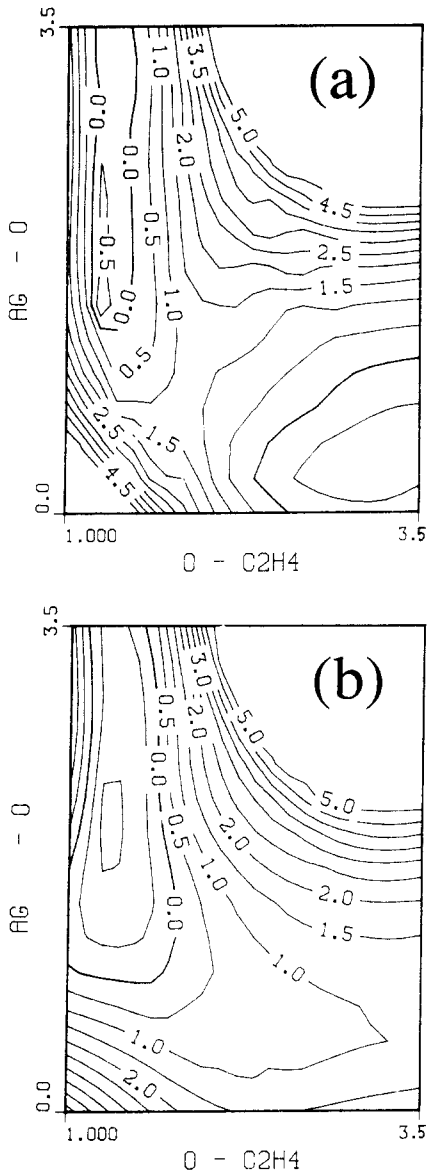

Figure 9. Contour plots of potential energy surfaces for the reaction to epoxide without (a) and with (9) subsurface oxygen. The silver-adsorbed oxygen (vertical axis) and adsorbed oxygen–ethylene (horizontal) distances are given in Å and the energies in eV. The zero of the energy scale is defined by the energy of silver + (isolated) epoxide. The plots are based on the calculations with Ag_4.

Figure 10 shows the calculated ethylene–oxygen interaction energies for the geometries of Figure 6a–c (in the absence of subsurface oxygen) as a function of the oxygen–carbon distance (for the case of Figure 6a, the distance between the oxygen and the middle of the carbon–carbon bond). This figure is based on calculations with Ag_4. Clearly, the interaction energy for the asymmetric geometries is less repulsive than that for the symmetric geometry of Figure 6a. Figure 11 shows COOP curves of the interactions between the ethylene π and (C–C antibonding) π^* orbitals and the oxygen and silver orbitals. In this figure, the geometries of Figure 6a,b are compared for silver–oxygen distance, 0.26 Å, and oxygen–ethylene distance, 2.1 Å. Now, when we go from the symmetric (Figure 6a) to the asymmetric (Figure 6b) geometry, we expect an *increase* of the overlap between the adsorbed O lone-pair orbital and the ethylene π^* orbital; in addition, we expect a *decrease* of the overlap between the O lone-pair and ethylene π orbitals. Figure 11b shows that, indeed, the bonding interaction with the ethylene π^* orbital increases a little. A more important effect, however, is the decrease of the antibonding interaction with the π orbital, as can be seen from Figure 11a. Apparently, the oxygen–ethylene repulsion can be considerably lowered by reducing the overlap between the ethylene π orbital

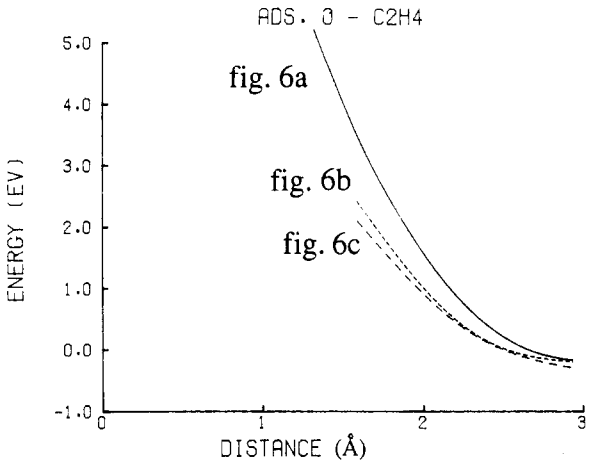

Figure 10. Interaction energy as a function of adsorbed oxygen–ethylene distance without subsurface oxygen, for the different geometries of Figure 6: Figure 6a (solid), Figure 6b (short dash), and Figure 6c (long dash).

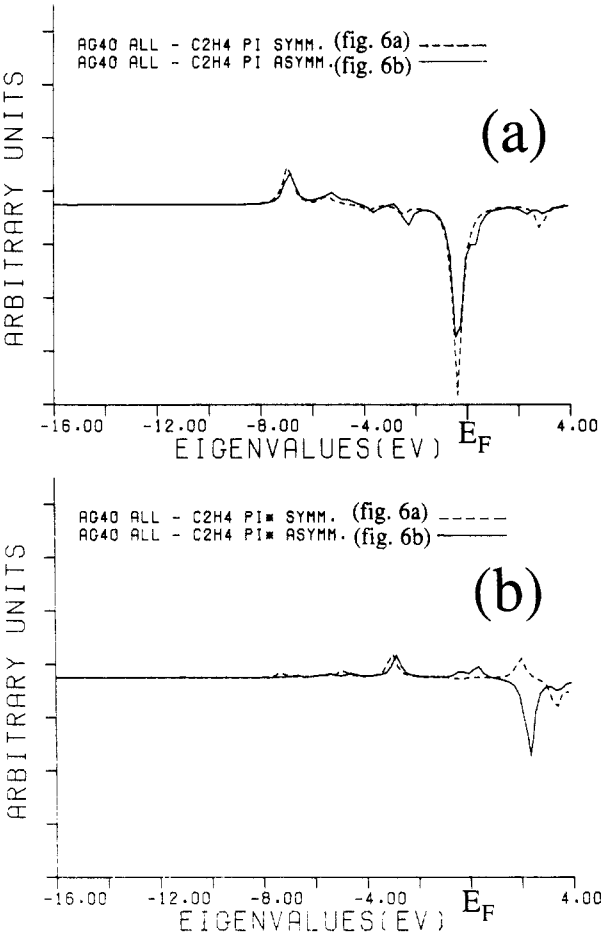

Figure 11. COOP curves of the interactions between ethylene and silver + adsorbed oxygen, in the absence of subsurface oxygen, for the geometries of Figure 6a (dashed) and Figure 6b (solid). The interactions with the carbon–carbon π-bonding (a) and π-antibonding (π^*) (b) orbitals are shown. The curves are based on calculations with Ag_4 with the oxygen–silver distance equal to the equilibrium distance and the oxygen–ethylene distance equal to 2.1 Å; note that these distances are different from the ones in Figure 8.

and oxygen and silver orbitals; this applies to the geometries both of Figure 6b and of Figure 6c. Note that this argument does not hold when subsurface oxygen is present, since in that case the strongly ethylene–oxygen antibonding levels are above E_F (see previous section).

For all three geometries of Figure 6, the filling of the C–C antibonding π^* orbital and the C–H antibonding orbitals was determined from a Mulliken population analysis. For none of the

three geometries did we observe any filling of C-H antibonding orbitals. This is not unreasonable, since these orbitals are high in the excited spectrum. However, the C-C antibonding π^* orbital, which has a much lower energy, does get partially filled. For example, for an ethylene-oxygen distance of 2.1 Å (see Figure 10), we found π^* occupations of 0.11, 0.18, and 0.08 electron for the geometries of Figure 6a, Figure 6b, and Figure 6c, respectively. The consequent C-C bond weakening may lead to C-C bond breaking, resulting in combustion. In the symmetric geometry of Figure 6a, also epoxide could be formed (the π^* occupation in epoxide is 0.5 electron). In this case, the weakening of the C-C bond is compensated for by the formation of two C-O bonds. When no subsurface oxygen is present, however, nonsymmetric attacks are energetically more favorable. Therefore, in this case, C-C bond weakening may take place without being compensated for by the formation of two C-O bonds (in fact, only one C-O bond is formed). This may explain the fact that, in the absence of subsurface oxygen, the rate of combustion is higher than in the presence of subsurface oxygen.[1]

4. Conclusions

Our calculations, in which the Ag(110) surface is modeled by finite clusters, show that subsurface oxygen enhances the reactivity to epoxide formation of chemisorbed oxygen. This increase in reactivity is a consequence of two effects. First, the chemisorption bond strength of oxygen decreases due to antibonding interaction with subsurface oxygen induced levels near E_F. Secondly, subsurface oxygen pushes part of the adsorbed O(2p) levels to higher energies. As a consequence, the adsorbed oxygen-ethylene strongly antibonding levels rise above the Fermi level. Therefore, the ethylene-oxygen interaction, which is repulsive in the absence of subsurface oxygen, becomes attractive when subsurface oxygen is present. The calculations with Ag_{10} + 2O suggest that, without subsurface oxygen, the ethylene-oxygen interaction is still repulsive when Ag(110) is covered with the high oxygen coverage of 0.5 monolayer. This repulsive interaction will largely inhibit geometries in which epoxide can be formed by oxygen insertion into the C-C double bond. Instead, in the absence of subsurface oxygen, ethylene will prefer to approach the adsorbed oxygen in geometries where the C-C π-bond orbital has little overlap with occupied oxygen orbitals. In these geometries, the probability for epoxide formation may be less, but partial filling of the C-C π-antibonding (π^*) orbitals could lead to an intermediate that leads to total combustion. In our calculations, we could not find any indication of direct C-H bond activation leading to combustion.

We wish to stress the importance of the role of the Fermi level in this catalytic process. It is to be expected that quite generally the presence of a Fermi level will lead to relief of the Pauli repulsion component of molecule-metal or molecule-adsorbate interactions as antibonding states rise above E_F. This has also been pointed out by other authors.[19,26] In this respect metals, and as a corollary heterogeneous catalysis, are very different from isolated transition-metal complexes, viz., homogeneous catalysis.

Acknowledgment. We thank the Dutch Committee for the Use of Supercomputers for providing financial support for the calculations. This work is part of the research program of the Netherlands Foundation for Fundamental Research on Matter (Stichting voor Fundamenteel Onderzoek der Materie) and was made possible by financial support from the Netherlands Organization for Scientific Research (Nederlandse Organisatie voor Wetenschappelijk Onderzoek).

Registry No. Ag(110), 7440-22-4; ethylene, 74-85-1; atomic oxygen, 17778-80-2.

(26) Sung, S.-S.; Hoffmann, R. *J. Am. Chem. Soc.* **1985**, *107*, 578. Raatz, F.; Salahub, D. R. *Surf. Sci.* **1986**, *176*, 219.

Thermal Behavior of Langmuir-Blodgett Films. 1. Electron Diffraction Studies on Monolayers of Cadmium Stearate, Arachidate, and Behenate

Johann E. Riegler†

AT&T Bell Laboratories, P.O. Box 900, Princeton, New Jersey 08540 *(Received: December 15, 1988; In Final Form: March 21, 1989)*

Electron diffraction patterns of monolayers of several cadmium fatty acid salts were studied as a function of the sample temperature. A sharp decrease of the diffraction peak intensities at temperatures well below the main melting temperature of the headgroup lattice indicates a pretransitional disordering. It depends on the chain length and starts at ~35 °C for cadmium stearate, at ~55 °C for cadmium arachidate, and at ~75 °C for cadmium behenate. The hexagonal geometry of the diffraction patterns does not change with temperature, and the radial and angular full width at half-maximum increase only slightly compared to the pronounced decrease of the intensity. This indicates that the *overall* bond orientational and translational order of the molecules is preserved and that the intensity decrease is caused by thermally induced random tilt orientational disorder or bending of the chains.

Introduction

Langmuir-Blodgett films are generated by transferring a preformed, water-supported monolayer of amphiphilic molecules onto a solid substrate. The organization of the molecules is controlled by the various interactions between their hydrophobic and hydrophilic parts and the interactions with the supporting substrate. Therefore, the ordering of the molecules and the phase behavior of the films can be expected to be rather complex, and many experimental and theoretical studies on water-supported

†Current address: Institut f. Physikalische Chemie, Universität Mainz, Welder-Weg 11, D-6500 Mainz, FRG.

0022-3654/89/2093-6475$01.50/0